Quarterly Journal of the
Royal Meteorological Society
RMetS

Cyclone intensification in the Kuroshio region and its relation to the sea surface temperature front and upper-level forcing

Leonidas Tsopouridis | Clemens Spensberger | Thomas Spengler

Geophysical Institute, University of Bergen, and Bjerknes Centre for Climate Research, Bergen, Norway

Correspondence
L. Tsopouridis, Geophysical Institute, University of Bergen, Bergen, Norway.
Email: leonidas.tsopouridis@uib.no

Abstract

The Northwest Pacific features strong sea surface temperature (SST) gradients providing favourable conditions for wintertime cyclone intensification in the midlatitudes. To estimate the relative contribution of the SST front to the evolution of cyclones and identify the mechanisms for cyclone intensification, we track individual cyclones and categorise them depending on their propagation relative to the SST front. We focus on cyclones remaining on either the cold or warm side of the SST front, as well as those crossing the SST front from the warm to the cold side. Cyclones crossing the SST front or remaining on its warm side propagate near the left exit region of the jet and are associated with higher precipitation, consistent with higher moisture availability and cyclone intensity. Comparing the different cyclone categories, there is no direct effect of the SST front on cyclone intensification. However, the SST front contributes to the climatological low-level baroclinicity, providing a conducive environment for cyclone intensification for the cyclones crossing the SST front. Compared with the Gulf Stream region, the land–sea contrast plays a less prominent role for the low-level baroclinicity in the Kuroshio region.

KEYWORDS
cyclone intensification, extratropical cyclones, jet stream, Kuroshio Extension, low-level baroclinicity

1 | INTRODUCTION

The Kuroshio and the Gulf Stream are the western boundary currents in the North Pacific and North Atlantic, respectively, and are associated with maxima in midlatitude air–sea heat exchange along the sea surface temperature (SST) front (Ogawa and Spengler, 2019). Both boundary-current regions are areas of frequent cyclogenesis (Hoskins and Hodges, 2002; Nakamura *et al.*, 2004), where a sum of processes favours storm development (Roebber, 1989). Upper-level forcing (e.g., Sanders and Gyakum, 1980; Uccellini *et al.*, 1984; Sinclair and Revell,

---

2000), low-level baroclinicity (e.g., Sanders, 1986; Wang and Rogers, 2001), and diabatic processes (e.g., Kuo *et al.*, 1991; Fink *et al.*, 2012; Chagnon and Gray, 2015) have been identified as the main mechanisms influencing the development of extratropical cyclones (hereafter cyclones: e.g., Petterssen and Smebye, 1971; Uccellini *et al.*, 1984; Nuss and Anthes, 1987). In this study, we will clarify the role of these mechanisms for cyclone intensification in the Kuroshio region, with a particular focus on the role of the SST front.

While the Kuroshio Extension and the Gulf Stream region have several characteristics in common, there are some important differences. For example, the Kuroshio is located further away from the Asian continent than the Gulf Stream from the North American continent. In addition, the characteristics of the wintertime upper-level jet differ considerably, with the Pacific jet being stronger and more confined meridionally at comparatively lower latitudes than the Atlantic jet (Spensberger and Spengler, 2020). We will clarify the extent to which these differences affect the cyclogenetic forcing in the Kuroshio Extension region.

Low-level temperature gradients, arising from either horizontal differences in the SST or due to the land–sea contrast, increase the low-level baroclinicity and thus facilitate cyclone intensification. Recent studies highlighted the role of the SST front in determining the wintertime low-level baroclinicity along the western boundary currents (e.g., Hotta and Nakamura, 2011; Papritz and Spengler, 2015). Here, the SST gradient both anchors the storm track (Nakamura *et al.*, 2008) and triggers convection and precipitation (Minobe *et al.*, 2008; Parfitt *et al.*, 2016; Vannière *et al.*, 2017). In addition to SST anomalies around the Gulf Stream and Kuroshio SST front, the comparatively cold North American land mass can also affect low-level baroclinicity strongly in winter (Nakamura and Yamane, 2009). Previous studies confirmed that the land–sea contrast contributes considerably to low-level baroclinicity in the Gulf Stream region (e.g., Cione *et al.*, 1993; Inatsu *et al.*, 2000; Wang and Rogers, 2001; Brayshaw *et al.*, 2009; Tsopouridis *et al.*, 2020) and also rapidly developing cyclones over the Northwestern Pacific have been associated with cold continental airmasses (Yoshida and Asuma, 2004).

Yoshida and Asuma (2004), however, also identified the strong and zonal upper tropospheric jet stream as a contributor to cyclogenesis in the Kuroshio region. Indeed, Jacobs *et al.* (2008) attribute up to 74% of the variance in deepening to differences in upper-level forcing. Cyclogenesis is fundamentally linked to the occurrence of jets (e.g., Sanders and Gyakum, 1980; Uccellini *et al.*, 1984; Schultz *et al.*, 1998; Sinclair and Revell, 2000), because the baroclinicity associated with the jet stream provides a source of

energy for cyclone intensification (Riviere and Joly, 2006). Rapid intensification of cyclones typically occurs in the left-exit region of jet streams (Uccellini, 1990), which is associated with enhanced upper-level divergence yielding vortex stretching (e.g., Ritchie and Elsberry, 2003; Oruba *et al.*, 2013).

In addition to low-level baroclinicity and upper-level forcing, diabatic heating associated with surface fluxes and latent heat release can contribute to cyclone intensification (e.g., Kuo *et al.*, 1991; Reed *et al.*, 1993; Nakamura *et al.*, 2004). With the Kuroshio Extension region featuring the highest surface heat fluxes in the wider North Pacific region (e.g., Josey *et al.*, 1998; Ogawa and Spengler, 2019), it is not surprising that strong surface heat and moisture fluxes significantly influenced the deepening of a Pacific cyclone that experienced weak upper-level forcing (Reed and Albright, 1986). Using numerical simulations, Kuwano-Yoshida and Asuma (2008) indeed found that latent heat release is important for the rapid intensification of cyclones over the Northwestern Pacific Ocean. Further, Hirata *et al.* (2018) demonstrated that surface fluxes can affect the intensity of an explosive cyclone and its bent-back front. However, the effect of surface fluxes remains small compared with other influences such as latent heat release (Reed *et al.*, 1993).

We perform a synoptic analysis to elucidate the different contributions of the aforementioned mechanisms to cyclone intensification in the Kuroshio region, where we focus on wintertime cyclones with maximum intensification in the Kuroshio Extension region. To evaluate the significance of the SST front on cyclone growth, we categorise these cyclones depending on their trajectories with respect to the SST front. Using these categories, we discuss the respective roles of upper- and lower-level forcing for cyclone intensification. We contrast our results for the Kuroshio Extension region with the Gulf Stream (documented by Tsopouridis *et al.*, 2020, hereafter TSS20), with special emphasis on similarities and differences between these regions.

2 | DATA AND METHODS

2.1 | Data

We use the ERA-Interim reanalysis data with a four-dimensional variational data assimilation scheme and a spectral truncation of T255 and 60 levels in the vertical (Dee *et al.*, 2011). We use fields pre-interpolated onto a 0.5° × 0.5° horizontal grid and 6-hr temporal resolution for the winter period (December–February) from 1979–2016.

For our analysis, we acquired the following data, in line with TSS20: mean sea-level pressure (MSLP),

RMetS

geopotential height at 300 hPa, sea surface temperature (SST), temperature at 850 hPa, total column water vapour (TCWV), vertically integrated water-vapour flux (IWVF), wind at 925 and 300 hPa, large-scale and convective precipitation, as well as latent and sensible surface heat fluxes. Surface heat fluxes and precipitation data are derived from the twice daily forecasts (initialized at 0000 and 1200 UTC) and are accumulated ± 3 hr around the respective timesteps (such as in Ogawa and Spengler, 2019).

2.2 | SST front

We identify the position of SST fronts using an objective frontal detection scheme. The scheme is based on the "thermal" method and has been used to detect atmospheric fronts (Jenkner *et al.*, 2010; Berry *et al.*, 2011; Schemm *et al.*, 2015). Further details are described in TSS20. To capture the most prominent SST fronts in the Kuroshio Extension region, we have chosen an SST gradient threshold of 1.25 K·100 km^{-1}. Our choice is based on a sensitivity analysis where we varied the threshold between 1.0 and 2.0 K·100 km^{-1} in steps of 0.25 K·100 km^{-1}. The chosen threshold is a trade-off between consistently detecting the main SST front, and avoiding too many detections of secondary SST gradient maxima as fronts. TSS20 used a larger threshold (2K·100 km^{-1}) for the Gulf Stream region, consistent with the stronger SST gradient in the Atlantic (e.g., Nakamura *et al.*, 2004). Our climatological SST front position coincides with the region of the maximum SST gradient, as presented in the SST climatologies of Yao *et al.* (2016), Tozuka *et al.* (2018), and Wang *et al.* (2019).

Following Masunaga *et al.* (2015), we divided the full period encompassing 38 winters into two time segments, prior to and after 2002, to assess the potential impact of the change in resolution of the SST in the ERA-Interim data on our results. Although the detected SST fronts are more variable after 2002, the mean position of the SST fronts, the SST distribution, and the propagation of cyclones relative to the SST front remain consistent across the time segments (see Appendix Figure A1). Further, the evolution of cyclone characteristics, assessed by separate composite analyses for the two time segments (not shown), is qualitatively unchanged. Thus, in line with Ogawa and Spengler (2019), we only present the results for the entire period from 1979–2016 (SST front climatology in Figure 1a). The unit of the SST front distributions in Figure 1a is a result of a normalisation to account for variations in the size of a grid cell. We thus sum the total length of all front lines within a given grid cell and divide this quantity by the number of time steps and the size of the grid cell.

2.3 | Jet stream detection

In order to assess the potential impact of upper-level forcing, we diagnose the upper-level flow for the cyclones in our database. This is also motivated by the North Pacific jet occurring most frequently slightly to the south of the Kuroshio Extension region (orange shading in Figure 1a), consistent with previous climatologies (e.g., Riehl *et al.*, 1954; Nakamura, 1992; Jaffe *et al.*, 2011; Spensberger and Spengler, 2020). The presented jet position is based on automatically detected jet axes, following the method and criteria of Spensberger *et al.* (2017) identifying lines separating cyclonic from anticyclonic wind shear on the 2-potential vorticity unit (PVU) surface (where 1 PVU $= 10^{-6}$ m^2·s^{-1}·K·kg^{-1}). The unit of the jet axis distributions is the result of the same normalisation process applied for the SST front distributions, as described in Section 2.2.

2.4 | Cyclone detection and tracking

We utilize the University of Melbourne cyclone detection and tracking algorithm (Murray and Simmonds, 1991a; 1991b). The algorithm detects maxima in the Laplacian of the MSLP field and tracks them over time, employing a nearest-neighbour method together with the most likely direction of propagation (Murray and Simmonds, 1991a; 1991b; Michel *et al.*, 2018, TSS20).

Analogous to the analysis for the Gulf Stream region in TSS20, we apply a number of track selection criteria. We require cyclones to propagate for at least 12 hr (three consecutive time steps) in the Kuroshio Extension region (30–50°N and 145–170°E), henceforth referred to as the "Kuroshio region". The minimum in the evolution of the surface pressure along the track must occur during December–February (DJF) and we only include tracks with maximum intensification, defined as the most rapid decrease in MSLP, in the Kuroshio region. Moreover, we require the great circle distance between cyclogenesis and cyclolysis to be greater than 300 km to remove quasistationary systems.

2.5 | Classification of cyclone tracks based on their position relative to the SST front

We identify the shortest distance between each cyclone position and the SST front for every timestep along the cyclone track and define a vector **r** pointing from the SST front to the cyclone. The orientation of **r** relative to the SST gradient ∇SST at the SST front allows us to classify the cyclone position relative to the SST front, with $\mathbf{r} \cdot \nabla$SST < 0
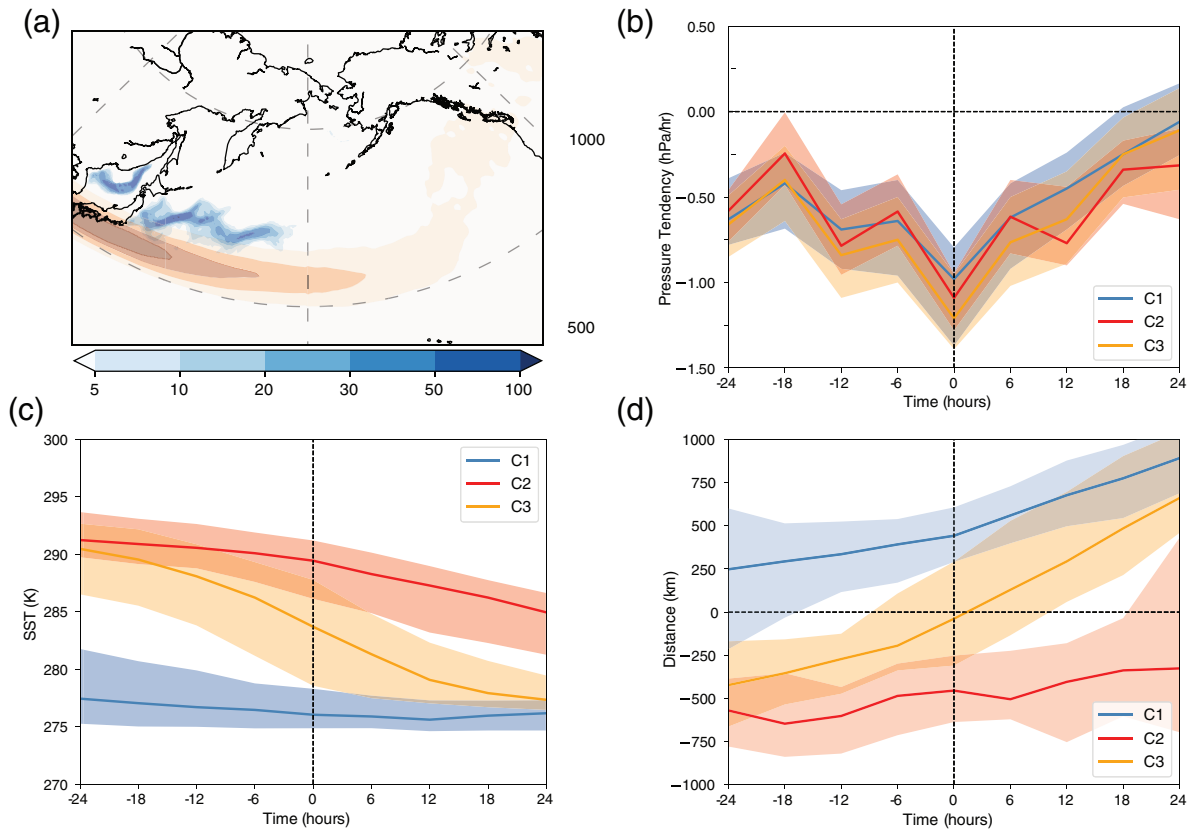
FIGURE 1 (a) SST front distributions (blue shading, km of line $(100\,\text{km})^{-2}$) and jet axis distributions (orange shading, km of jet axis line $(1{,}000\,\text{km})^{-2}$) for the North Pacific. The Kuroshio region is marked with a red box. (b) Pressure tendency (hPa·hr^{-1}) for the three categories relative to the time of maximum intensification. Lines indicate the median and the shading the interquartile range. (c) As (b), but for the SST. (d) Distance (km) between cyclone centres and the SST front relative to the time of maximum intensification

on the cold side of the SST front and vice versa on the warm side. Further details are described in TSS20. With the positions of both the SST fronts and the cyclone tracks, we follow TSS20 and categorize the propagation of cyclones relative to the SST fronts only within the Kuroshio region (red rectangle in Figure 1a) into five categories. In category C1, cyclones always remain on the cold side of the SST front, whereas for category C2 cyclones always stay on the warm side of the SST front. In category C3, cyclones are crossing the SST front from the warm to the cold side, contrarily to category C4, in which cyclones cross the SST front from the cold to the warm side. Finally, cyclones that belong to category C5 cross the SST front multiple times.

3 | RESULTS

3.1 | Cyclone occurrence and intensification

Analogously to TSS20 for the Gulf Stream region, we restrict our focus to categories C1, C2, and C3 during the

winter season (DJF) over the North Pacific Ocean. Category C4 comprises only 28 cyclones that cross the SST front from the cold to the warm side, making it challenging to deduce statistically robust results. As cyclones in C5 cross the SST front multiple times, it is impossible to diagnose the role of the SST front in the cyclone evolution. However, 142 cyclones consistently stay on the cold side (C1, Figure 2a), 97 cyclones stay on the warm side (C2, Figure 2b), and 188 cyclones cross from the warm to the cold side (C3, Figure 2c). For these three categories, the cyclones all propagate from the southwest to the northeast. Cyclones in C1 and C3 remain closer to the Asian continent than the ones in C2, which propagate northwards the least (Figure 2b).

Amongst these three categories, cyclones in C3 deepen the most from 12 hr prior to maximum intensification to 6 hr after, undergoing a maximum six-hourly deepening corresponding to 30 hPa·day^{-1} (median in Figure 1b). Cyclones in C2 intensify slightly more slowly compared with C3, with a maximum deepening rate corresponding to approximately 26 hPa·day^{-1}. From 12 hr after maximum intensification onward, however, C2 becomes the category
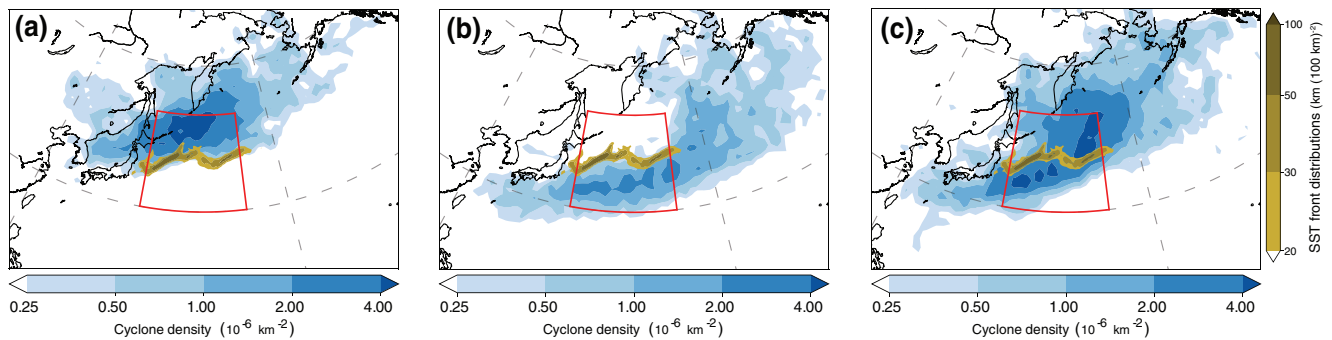
FIGURE 2 (a) Cyclone density for category C1 (blue shading, 10^{-6} km^{-2}) based on the ERA-Interim reanalysis for the winter seasons in 1979–2016 for cyclones with maximum intensification in the Kuroshio region. Density of the SST fronts (brown shading, km of line(100km)$^{-2}$) as in Figure 1, but for the most prominent SST fronts in the Kuroshio region. (b,c) As (a), but for categories C2–3, respectively. See main text for more details on the cyclone detection and categorisation

that deepens the most (median in Figure 1b). Cyclones in C1 intensify least, with a maximum deepening rate corresponding to 22 hPa·day^{-1}. Based on the definition of Sanders and Gyakum (1980), 13.5% of the cyclones in C1 (19 cyclones), 17.5% of the cyclones in C2 (17 cyclones), and 21% of the C3 cyclones (40 cyclones) are explosive. The higher percentages for C2 and C3 are consistent with the study of Iwao *et al.* (2012), who found that the majority of explosive cyclones in the Kuroshio region originate southwest of Japan (Figure 2b,c).

The intensification for the different categories is different compared with the Gulf Stream region, where cyclones in C2 were shown to intensify considerably less than those in C1 and C3 (TSS20). Further, in the Gulf Stream region, 23% of cyclones in C1 and 40% of cyclones in C3 are explosive, compared with 13.5 and 21%, respectively, in the Kuroshio region. Despite the overall lower fraction of explosive cyclones in the Pacific, 17.5% in C2 cyclones in the Kuroshio region are explosive, compared with 11% in the Gulf Stream region.

The higher percentage of explosive cyclones in the Gulf Stream region for C1 and C3 compared with the Kuroshio region could be associated with the additional low-level baroclinicity in the Atlantic due to the land–sea contrast (TSS20). During the early stages, cyclones in C1 and C3 in the Gulf Stream region propagate closer to the cold continental landmass, which enhances the low-level baroclinicity (TSS20). Conversely, cyclones in C1 and C3 in the Kuroshio region are further away from the continent and thus have a more maritime character and weaker low-level baroclinicity. With diabatic processes playing a key role for explosive cyclogenesis, precipitation and latent heat fluxes could also play a crucial role.

However, a higher fraction of C2 cyclones in the Pacific are associated with explosive cyclogenesis compared with those propagating in the Gulf Stream region, despite the

similar distribution of surface heat fluxes and the propagation over lower SSTs in the Pacific. We suggest that the reason for the higher explosive fraction for C2 cyclones in the Pacific is the proximity of cyclones to a stronger upper-level jet (Figure 1a) compared with the Gulf Stream region (cf. TSS20).

To estimate the possible effect of the SST front on cyclone intensity, we present its distribution in Figure 3. The location of the maximum intensity is rather equally spread on the cold side of the SST front for C1 and C3, with the latter being closer to the main SST gradient (Figures 1a and 3a,c) and associated with the highest peak intensity among the three categories (not shown). For cyclones of C1 and C3, the location of maximum intensity is close to the location of maximum intensification (not shown). Similarly to C3, cyclones of C2 are also characterized by higher intensity than those in C1 (Figure 3b), but they reach their maximum intensity further downstream, similar to the Atlantic C2 cyclones (TSS20).

3.2 | Cyclone-relative SST and wind composites

We present cyclone-relative composites for the first three categories around the time of maximum intensification to better understand the role of the different forcing mechanisms in the Kuroshio region.

For C1, cyclones propagate over comparatively low SSTs (approximately 277 K) throughout their evolution (Figure 1c), as cyclones remain on the cold side of the SST front (Figure 1d). Over time, cyclones gradually propagate away from the SST front over even lower SSTs (Figure 4a–c). Compared with C1, cyclones in C2 propagate over approximately 15 K higher SSTs (Figure 1c), although SSTs are still about 4 K lower compared with
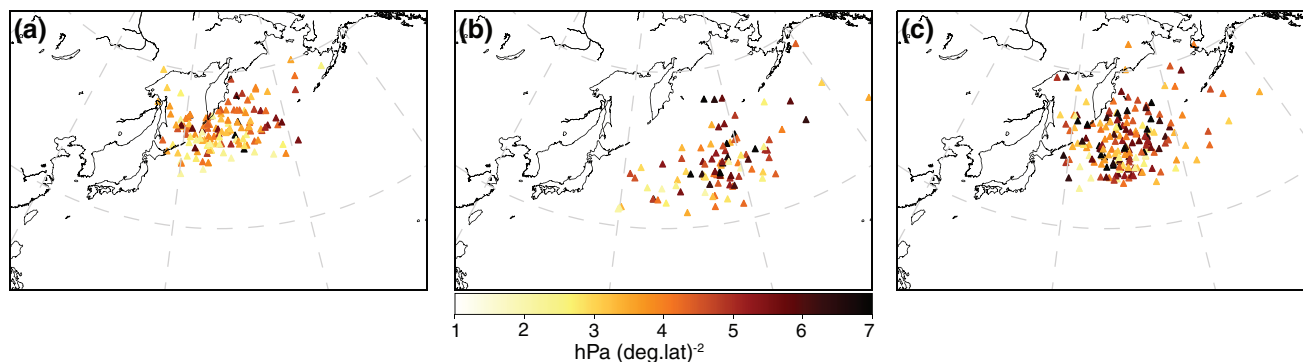
FIGURE 3 (a) Maximum Laplacian of the MSLP (hPa·(deg lat)$^{-2}$) for cyclones in C1. (b,c) As in (a), but for cyclones in C2 and C3, respectively

cyclones in C2 in the Atlantic (TSS20). However, 12 hr after maximum intensification, cyclones in C2 propagate over slightly lower SSTs (Figure 4f), consistent with the cyclones getting closer to the SST front (Figure 1d).

C3 can be seen as a combination of C1 and C2. Prior to the time of maximum intensification, cyclones propagate on the warm side of the SST front (Figure 1d) and thus over higher SSTs (Figures 1c and 4g). After crossing the SST front around the time of maximum intensification (Figures 1d and 4h), cyclones propagate gradually over lower SSTs (Figures 1c and 4i). The cross-frontal SST difference in C3 is, however, less sharp than the one observed in the Gulf Stream region (TSS20), due to a more spatially confined SST front in the Gulf Stream compared to the Kuroshio region (e.g., Nakamura *et al.*, 2004).

For all categories, the maximum wind at 925 hPa increases gradually throughout the cyclone development. This increase is more apparent in C2 and C3, with the wind speed increasing from 18 to 27 m·s^{-1} within 24 hr (Figure 4d–i), compared with C1, where there is an increase of 6 m·s^{-1} (Figure 4a–c). Thus, in contrast to the Gulf Stream region, C2 cyclones are stronger on average than C1 cyclones (cf. TSS20). Nonetheless, in both the Pacific and the Atlantic, the maximum wind speed occurs in the south–southeast quadrant, due to the superposition of circulation these cyclones and their east–northeastward propagation.

Cyclones in C1 and C3 in the Kuroshio region develop in environments with about equally strong low-level baroclinicity (850-hPa temperatures in Figure 4a–c,g–i), while less low-level baroclinicity is observed for C2 (Figure 4d–f). The temperature gradient at 850 hPa is overall smaller compared with the Gulf Stream region for cyclones of categories C1 and C3, while being rather similar for C2 (cf. figure 4 in TSS20). Following the argument of TSS20, the higher low-level baroclinicity in the Gulf Stream region is most likely associated with the proximity of the cyclones to the cold continental landmass. Their argument

is consistent with our results for the Kuroshio region, where cyclones are located further away from the cold-air reservoir over the Asian continent and exhibit weaker low-level baroclinicity.

3.3 | Cyclone-relative surface heat flux composites

For all three categories, upward surface heat fluxes dominate around the cyclones (Figure 5). The sensible heat fluxes are largest in the southwest quadrant on the warm side of the SST front, yielding a larger atmosphere–ocean temperature contrast. Averaged over the composite domain, cyclones in C2 are associated with higher sensible heat fluxes (Figure 5d–f) than those in C1 (Figure 5a–c), due to the propagation over higher SSTs (Figure 1c). Similarly to the sensible heat fluxes, the latent heat fluxes are also higher in the southwest quadrant, with the maximum values appearing slightly to the south of the sensible heat fluxes (consistent with, for example, figure 6a,b in Rudeva and Gulev, 2011). This offset in the location of the flux maxima is most likely associated with the saturation mixing ratio increasing exponentially with increasing SSTs following the Clausius–Clapeyron relation.

Sensible and latent heat fluxes follow a distribution for all three categories very similar to that in the Gulf Stream region, except that the amplitude of the fluxes is larger in the Atlantic (cf. TSS20). This is most likely attributable both to the SST gradient being larger in the Gulf Stream compared with the Kuroshio Extension and to cyclones being located closer to the SST front during the time of maximum intensification.

At 12 hr prior to maximum intensification, cyclones in C3 are still located on the warm side of the SST front and consequently feature intense latent and sensible heat fluxes exceeding 280 and 120 W·m^{-2}, respectively
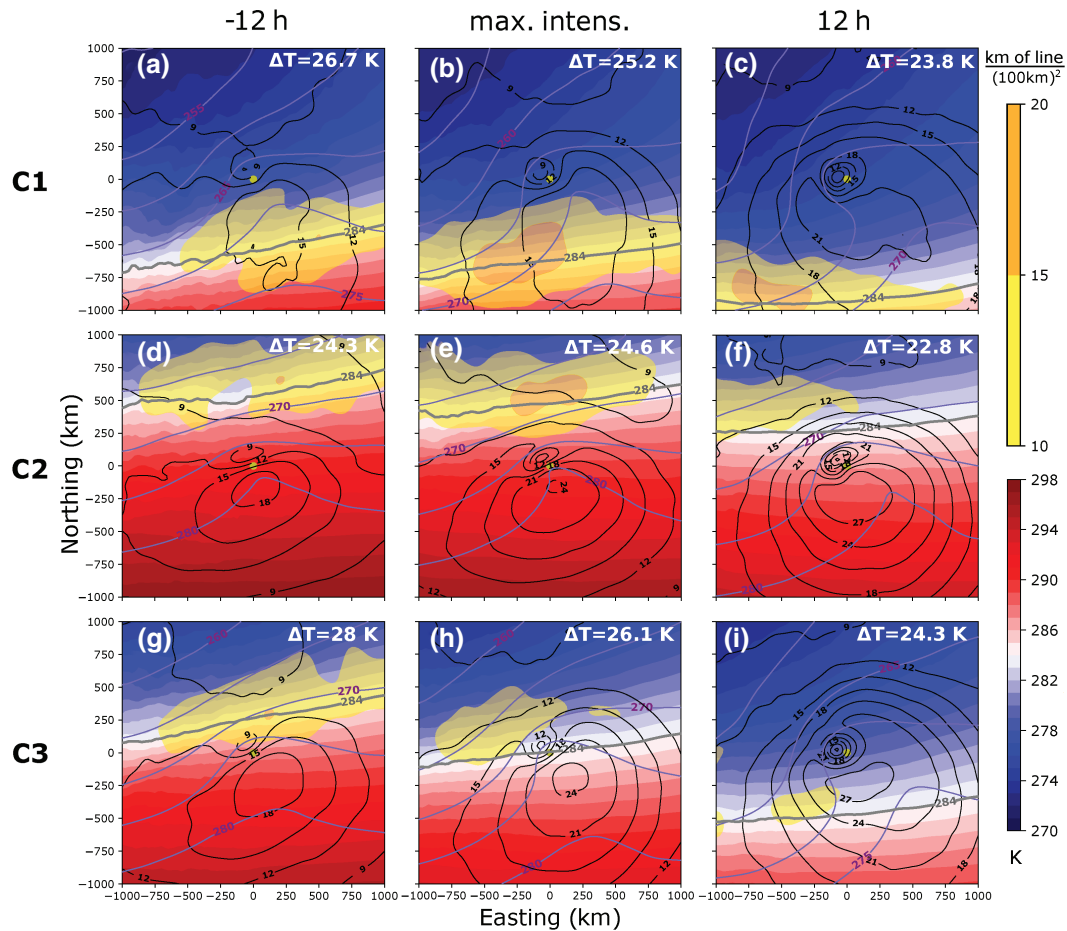
FIGURE 4 Composite evolution of cyclone-centred SST (blue–red shading, K), temperature at 850 hPa (purple contours, interval: 5 K), wind speed at 925 hPa (black contours, interval: 3 m·s^{-1}), and SST front density (yellow shading, in 10^{-5} km^{-1}). The isotherm of 284 K (grey contour) estimates the position of the SST front. Numbers in the top right of each panel represent the temperature difference at 850 hPa in the composite domain. Left, middle, and right panels are for 12 hr prior to maximum intensification, maximum intensification, and 12 hr after maximum intensification, respectively. Top, middle, and bottom panels show the categories C1, C2, and C3, respectively

(Figure 5g). At this point in time, both latent and sensible heat fluxes are even slightly higher than for cyclones in C2. Considering the relatively similar wind speeds between the two categories, the higher surface heat fluxes in C3 compared with C2 can be related to the closer proximity of cyclones to the SST front (Figure 1d). During the development, the amplitude of the surface heat fluxes remains more or less unchanged, but the location shifts southwards as cyclones in C3 move away from the SST front. At the same time, downward sensible heat fluxes appear to the east of the cyclone core (Figure 5i).

For all three categories, the highest upward sensible heat fluxes occur in the west–southwest quadrant and are associated with cold-air advection across the SST front (consistent with Vannière *et al.*, 2017). While latent heat fluxes are directed upwards throughout the evolution, sensible heat fluxes can also be directed towards the ocean within the cyclones' warm sector (Figure 5). For C1, a small area of downward sensible heat fluxes

appears during the maximum intensification in the southeast quadrant, due to warm-air advection over relatively lower SSTs (Figure 5b). Downward fluxes for C2 only occur in a small region 12 hr after maximum intensification. As the cyclone and its warm sector remain on the warm side of the SST front, the warm air only marginally exceeds the SST in some locations. Once the cyclone crosses the SST front, downward fluxes appear more widespread for C3 (Figure 5i), but remain weak. Overall, the dipole structure becomes more apparent for C2 and C3 at 12 hr, due to the higher intensity of cyclones compared with C1 (Figure 4). Thus, stronger cyclones feature more pronounced dipole structures in surface heat fluxes.

Downward sensible heat fluxes to the east of the cyclone core are more pronounced in the Gulf Stream region throughout the evolution in C1, and after maximum intensification for C3 (TSS20). We relate these more pronounced downward fluxes in the Atlantic to the sharper SST front in the Gulf Stream region, increasing
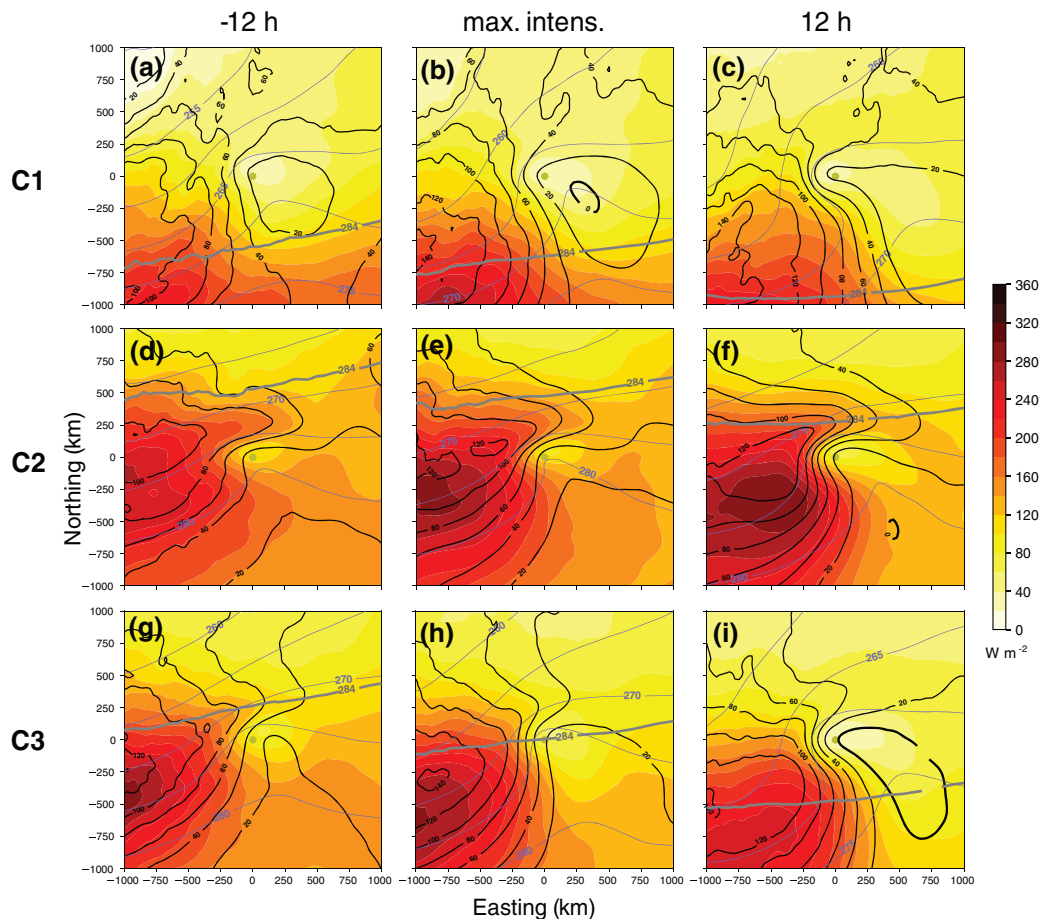
FIGURE 5 Composite evolution of cyclone-centred latent heat fluxes (yellow–red shading, W·m^{-2}), sensible heat fluxes (black contours, thick line for the zero contour, interval: 20 W·m^{-2}), and temperature at 850 hPa (purple contours, interval: 5 K). Panel setup and SST front position ($T = 284$ K) as in Figure 4

the likelihood that warm air originating from the south reverses the air–sea temperature contrast. Brayshaw *et al.* (2009) showed that the orientation of the North American continent increases the low-level baroclinicity by amplifying the pool of cold continental air to the east. Analogous to their argument for the Atlantic, we suggest that the more tilted SST front in the Gulf Stream region, compared with the Kuroshio region, could further contribute the amplification of temperature differences across the SST front and thus lead to more pronounced downward sensible heat fluxes to the east of the cyclone core, as documented for the Gulf Stream region (TSS20). For C2, the dipole is roughly similar in both regions. Nonetheless, in the Gulf Stream region it becomes more apparent at 12 hr, due to cyclones propagating closer to the SST front than in the Kuroshio region (TSS20).

Overall, the highest sensible heat fluxes are located close to the SST front on its warm side and the highest fluxes occur during maximum intensity of the cyclones. This is consistent with the study of Rudeva and Gulev (2011), which highlights that the SST front determines the

location of the maximum surface heat fluxes, whereas the cyclones' intensity regulates when the maximum fluxes will occur.

3.4 | Cyclone-relative moisture composites

C2 is the category with the highest values of TCWV (hereafter moisture content), exceeding 27 kg·m^{-2} at all time steps shown and peaking at maximum intensification (Figure 6e), also featuring the strongest IWVF (hereafter moisture transport) (Figure 6d–f). This is not unexpected, as cyclones in C2 stay on the warm side of the SST front, where the large amount of moisture can be explained by the Clausius–Clapeyron relation.

For C1, the highest moisture content occurs prior to maximum intensification (between −12 and 0 hrs), reaching 21 kg·m^{-2} (Figure 6a,b) nearly 1,000 km to the south of the cyclone centre. At 12 hr after maximum intensification, the maximum moisture content decreases by about

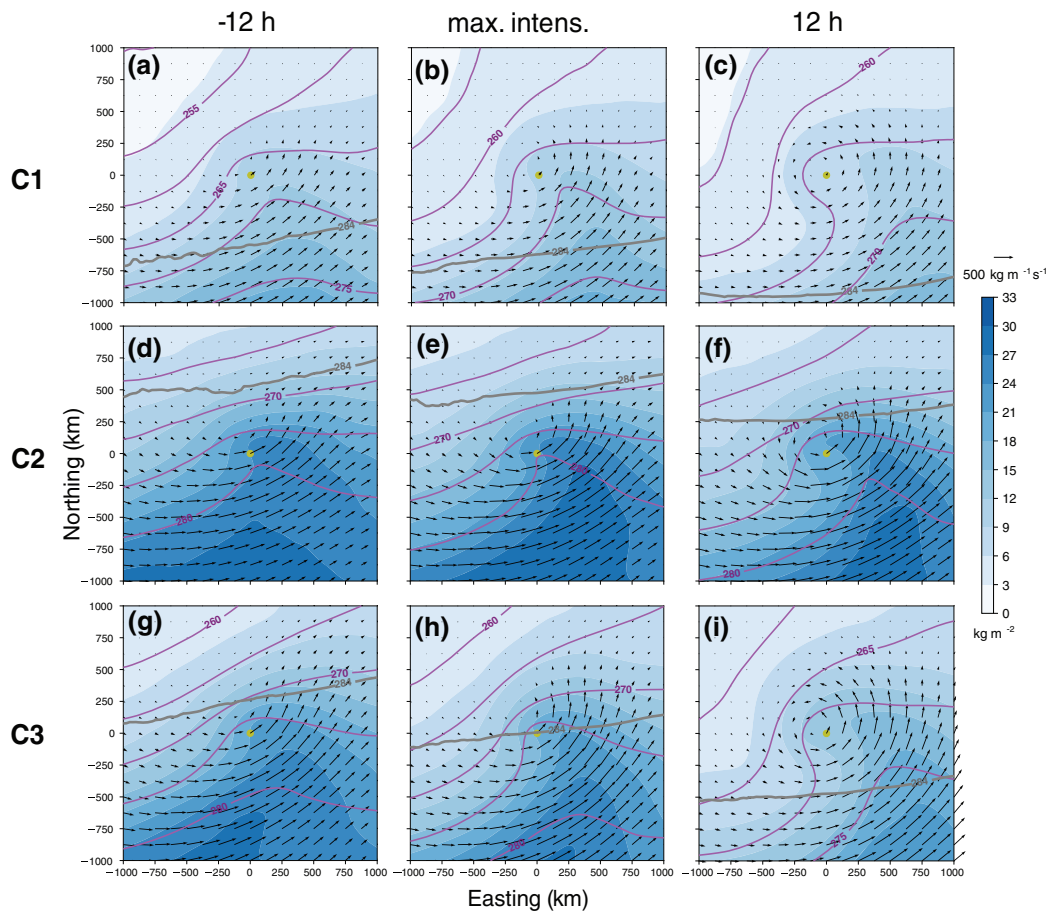**FIGURE 6** Composite evolution of cyclone centred total column water vapour (blue shading, kg·m^{-2}), integrated water vapour flux (black vectors), and temperature at 850 hPa (purple contours, interval: 5 K). Panel setup and SST front position as in Figures 4 and 5

3 kg·m^{-2} and is now located near the southeastern corner of the composite domain (Figure 6c). We relate this gradual reduction in moisture to the propagation of cyclones to the northeast (Figure 2a), moving at a greater distance from the SST front during the evolution of C1 cyclones (Figure 1d).

For C3, the moisture content peaks initially between 27 and 30 kg·m^{-2} at a distance of 750 km to the south of the cyclone centre (Figure 6g). This maximum gradually decays as the cyclones propagate towards the cold side of the SST front (Figure 6g–i), with a corresponding shift of the maximum towards the southeastern sector of the cyclone. The largest moisture transport occurs during maximum intensification in C3 (Figure 6h).

For all three categories, we note the development of a cyclonic wrap-up of both moisture content and transport around the cyclone core, which is progressively more evident throughout the cyclone development (Figure 6). The wrap-up of the warm sector is more distinct for C2 and C3 at 12 hr (Figure 6f,i), consistent with a higher cyclone intensity compared with C1 (cf. low-level wind speeds in Figures 3 and 4c,f,i).

The spatiotemporal evolution of moisture content and transport is similar for the Gulf Stream region. However, both moisture content and transport are consistently lower in the Kuroshio region compared with the Gulf Stream region (cf. TSS20). We relate these differences to the generally higher SSTs on the warm side of the Gulf Stream compared with the Kuroshio region. Due to this difference, Atlantic cyclones of all categories have on average a larger reservoir of moisture to tap into than Pacific cyclones.

3.5 | Cyclone-relative precipitation composites

C1 is the category with the lowest large-scale precipitation among the three categories and is characterized by a gradual yet minor increase of average large-scale precipitation during cyclone development (Figure 7a–c). Twelve hours past maximum intensification, cyclones in C2 are accompanied with on average about 2.5 mm·day^{-1} more intense large-scale precipitation compared with C1 (Figure 7c,f). Precipitation is thus consistent with the higher moisture
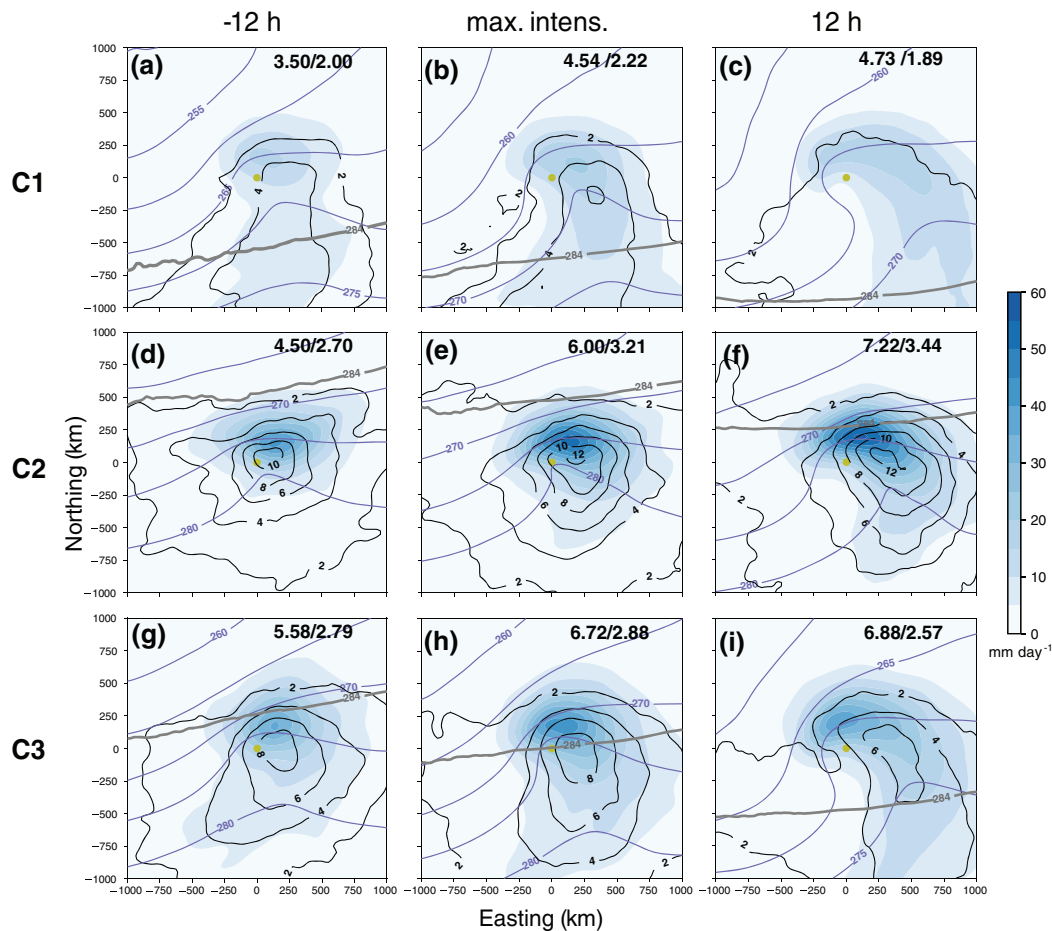
FIGURE 7 Composite evolution of cyclone-centred large-scale precipitation rate (blue shading, mm·day^{-1}), convective precipitation rate (black contours, mm·day^{-1}), and temperature at 850 hPa (purple contours, interval: 5 K). Panel setup and SST front position as in Figures 4–6. Numbers in the top right of each panel represent the average large-scale/convective precipitation in the composite domain

availability and cyclone intensity in C2 compared with C1.

The average large-scale precipitation in the Gulf Stream region was similar for C1 and C2, with the respective moisture availability being large for both categories, though slightly higher for C2 (TSS20). In the Kuroshio region, cyclones in C2 are stronger than those in C1 and associated with higher moisture content, resulting in the higher large-scale precipitation in C2 for the Kuroshio region.

Likewise, the convective precipitation is higher in C2 compared with C1 (Figure 7a–f). The maximum intensity of the convective precipitation for C2 occurs at a later stage of the development (0 hr and 12 hr), exceeding 12 mm day^{-1} approximately 200 km to the east of the cyclone core (Figure 7e,f). In C2, convective precipitation increases with cyclone intensity from 0 to 12 hr (Figure 7e,f), whereas for C1 it decreases for the same time period (Figure 7b,c). C1 thus shows that, in contrast to large-scale precipitation, convective precipitation does not necessarily increase with cyclone intensity. Conversely,

convective precipitation evolves in tandem with the SSTs around the cyclone, indicating that local evaporation plays an important role for convective precipitation (consistent with Hand *et al.*, 2014; Pfahl and Sprenger, 2016; TSS20).

In addition to the quantitative difference, the structure of precipitation is different for C1 and C2. The maximum convective and large-scale precipitation is located closer to the cyclone centre in C2 than in C1 (Figure 7a–f). The same spatial distribution of precipitation was also observed for the Gulf Stream region (TSS20), with higher precipitation for C1, due to cyclones propagating over slightly higher SSTs and associated with higher low-level baroclinicity than in the Kuroshio region.

In contrast to C1, cyclones in C2 propagate in the subtropics, over an area with both high SSTs (Figure 1c) and moderate, but still substantial, baroclinicity (Figure 4). Such an environment is favourable for the development of hybrid cyclones (e.g., Guishard *et al.*, 2009; Yanase *et al.*, 2014; Yanase and Niino, 2019). In particular, Yanase and Niino (2019) pointed out the presence of a convective core in hybrid cyclones, which would explain why the

precipitation in C2 is more confined around the cyclone centre. This interpretation is also consistent with Pfahl *et al.* (2015), who found that the precipitation band was located closer to the cyclone centre when increasing global mean surface temperature. In synthesis, all these results show that the absolute SST around the cyclone shapes the spatial distribution of precipitation around the cyclone centre.

C3 is associated with the highest average large-scale precipitation among the three categories up to maximum intensification (Figure 7g,h). There is a steady increase of average large-scale precipitation until maximum intensification with only a slight increase afterwards, whereas convective precipitation remains roughly unchanged up until the cyclones cross the SST front (Figure 7g,h) and decays slightly from 0h to 12 hr (Figure 7i). A similar decrease of convective precipitation was discussed before also for C1, despite the higher cyclone intensity. Thus, whereas large-scale precipitation evolves in tandem with cyclone intensity, the convective precipitation co-evolves more closely with the underlying SST.

The increase of large-scale precipitation over time is more pronounced for the Gulf Stream region, where stronger low-level baroclinicity leads to enhanced ascent along the steeper slopes of isentropic surfaces (cf. TSS20). Low-level baroclinicity is generally weaker in the Kuroshio region, such that this factor explains less of the observed differences and evolution of cyclones in the Kuroshio region. Instead, the increase in large-scale precipitation observed during the evolution of cyclones in C3 can mainly be explained by the higher cyclone intensity (Figures 4h,i and 7h,i). Further, the more intense precipitation for categories C2 and C3 compared with C1 follows from a combination of stronger cyclones and higher moisture content (Figure 7).

3.6 | Cyclone-relative geopotential and wind at 300 hPa

So far, we have attempted to explain cyclone intensification in terms of low-level baroclinicity and moisture availability. Cyclones in C3 have more low-level baroclinicity than cyclones in C2, which can explain their slightly faster intensification despite the fact that C2 has more moisture available. However, C1 is characterised by similar low-level baroclinicity as C3, but cyclones in C1 intensify considerably less. Moreover, cyclones in C2 intensify much faster in the Kuroshio than in the Gulf Stream region, despite similar baroclinicity and more available moisture in the Gulf Stream region. Therefore, we need to also consider upper-level forcing and the jet as a potential third

factor accounting for differences between our cyclone categories.

Cyclones in C1 propagate at a larger distance from the climatological position of the Pacific jet compared with C2 and C3 (Figures 1a, 2b,c). Consequently, the wind-speed maximum at 300 hPa is furthest away from the cyclone centre in C1 (Figure 8a–c). The wavy structure in both geopotential and wind suggests that cyclones are typically associated with an upper-level trough to the northwest of the cyclone. During the evolution in C1, the wind maximum shifts eastward (Figure 8b,c), following the development of the trough to the northwest (Figure 8a–c).

For C2, the isohypses are generally spaced more closely than in C1 (Figure 8a–f). Consistently, C2 is the category with the highest wind speed at 300 hPa, associated with a jet streak of $60–70 \, \mathrm{m \cdot s^{-1}}$, 750 km to the west–southwest of the cyclone centre 12 hr before maximum intensification (Figure 8d). Cyclones in C2 propagate close to the jet and stay in the left exit region of the jet throughout the evolution shown (Figure 8d–f). In contrast, in the Gulf Stream region, cyclones in C2 evolve at a greater distance from the climatological position of a weaker upper-level jet, compared with the Pacific, and are associated with the lowest wind-speed maximum at 300 hPa during maximum intensification among the three categories (TSS20).

As before, C3 can be interpreted as a combination in C1 and C2. Initially, the position relative to the jet is similar to C2 (Figure 8g), but during the evolution the cyclones propagate northward and away from the jet (Figure 8g,h). Twelve hours past maximum intensification (Figure 8i), the distribution of geopotential height and wind speed is approaching that in C1, with the presence of an upper-level trough in the northwest quadrant of the cyclone composite. Wind speeds remain higher in C3 than in C1, but at this point in time both wind maxima are located at a distance of more than 800 km to the south of the cyclone centre (Figure 8c,i).

Based on these results, it seems likely that upper-level forcing contributed to the more rapid deepening in C2 and C3 compared with C1 (Figure 1b). Up until the time of maximum intensification, cyclones in both C2 and C3 are located near the left exit of the jet (Figure 8d–i), whereas cyclones in C1 are further away from the jet (Figure 8a–c). The forced ascent at the left exit of the jet likely contributes to the more intense large-scale precipitation for C2 in the Kuroshio compared with the Gulf Stream region. The position relative to the upper-level jet thus appears to be an important contributor to cyclone intensification in the Kuroshio region and can explain the higher intensification of cyclones for C2 and C3 compared with cyclones in C1, as well as the higher intensification of C2 cyclones in the Pacific compared with the Atlantic. With C3 also
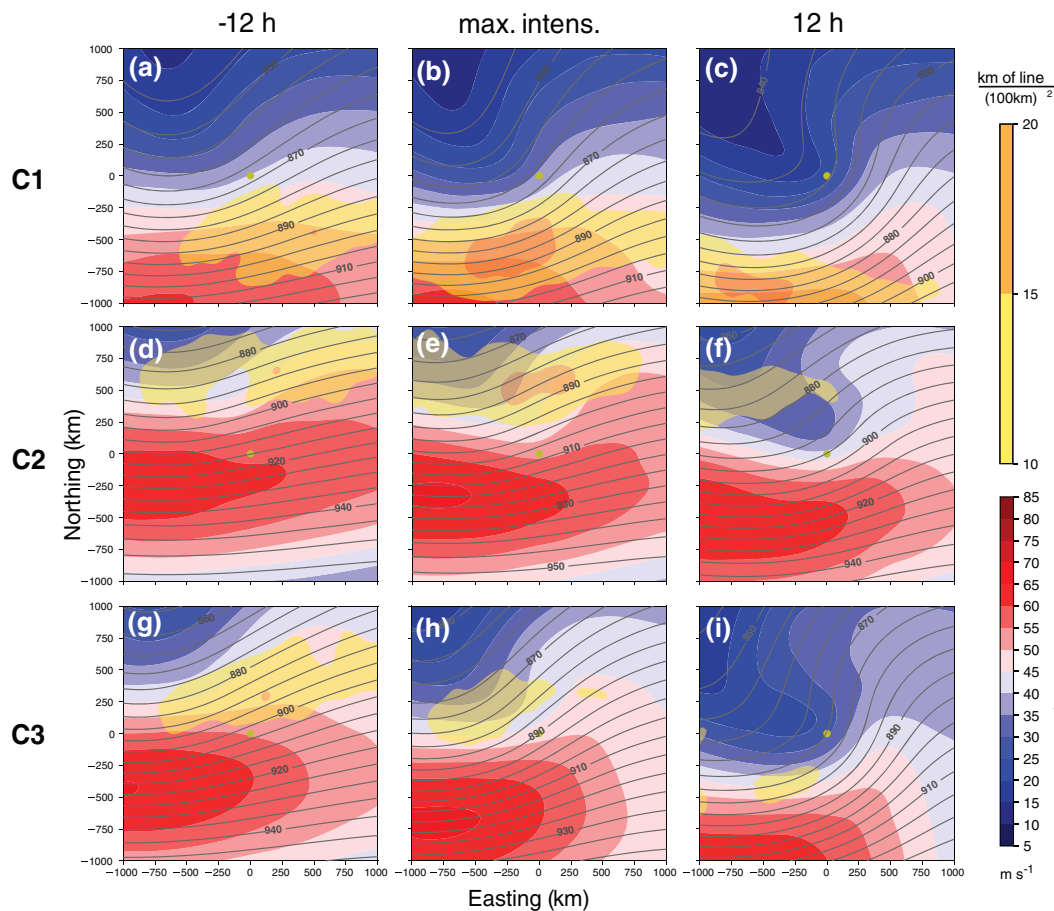
FIGURE 8 Composite evolution of cyclone-centred SST front density (yellow shading, in 10^{-5} km^{-1}), wind speed at 300 hPa (blue-red shading, m s^{-1}), and geopotential height at 300 hPa (grey contours, interval: 5 gpdm). Panel setup as in Figures 4–7

being associated with stronger low-level baroclinicity than C2 (see temperature gradient at 850 hPa in Figure 4d–i), the higher intensification of cyclones in C3 is related to a combination of both upper- and lower-level forcing.

4 | CONCLUDING REMARKS

We identified the main characteristics for categories of cyclones differing in their propagation relative to the SST front in the Kuroshio region. The SST front was detected automatically using an established algorithm and we considered cyclones remaining either on the cold (C1) or warm (C2) side of the SST front, as well as those crossing the SST front from the warm to the cold side (C3). We examined the potential role of the SST front in cyclone intensification and identified the mechanisms promoting cyclone intensification for these categories by compositing the evolution of these cyclones around their time of maximum intensification. As mechanisms, our analysis included low-level baroclinicity and upper-level forcing by the jet, as well as moisture transport and precipitation. The

results aid our understanding of the role of the SST front along the Kuroshio Extension for cyclone intensification and enable us to generalise the results of TSS20 for the Gulf Stream region to western boundary currents in general.

Cyclones on the warm side of the SST front (C2) deepen more rapidly compared with cyclones on the cold side (C1) (Figure 1b). This supports previous studies that demonstrated that higher SSTs can lead to more intense cyclones (e.g., Reed *et al.*, 1993; Hirata *et al.*, 2018). A comparison with C2 in the Gulf Stream region, however, demonstrates that this relation must be more complex, as Atlantic C2 cyclones propagate over even higher SSTs than the corresponding ones in the Kuroshio region, yet they intensify the least of all Atlantic categories and also less than Pacific C2. Further, in both the Kuroshio and the Gulf Stream region, cyclones in C3 intensify the most, although they consistently propagate over lower SSTs than those in C2. Given these discrepancies, our results suggest that, even if higher SSTs can affect the intensification of cyclones, this effect is secondary to other effects on synoptic time-scales.

Nevertheless, SSTs strongly modulate the local surface heat fluxes and convective precipitation, as well as

the climatological moisture availability. Cyclones on the cold side of the SST front have, on average, less moisture available and are associated with weaker surface fluxes. Consistent with the overall lower SSTs in the Kuroshio region compared with the Gulf Stream region, cyclones in the Kuroshio region are also, in general, associated with less convective precipitation.

We identified clear differences in the mechanisms responsible for cyclone intensification between the Kuroshio and the Gulf Stream region. Low-level baroclinicity is generally weaker around the Kuroshio than around the Gulf Stream. In addition, cyclones have, on average, less moisture available. Consequently, both low-level baroclinicity and moisture availability play a less important role for cyclone intensification in the Kuroshio region and account for a smaller part of the differences between the categories. Even though the SST contrast across the Kuroshio is weaker than across the Gulf Stream, we mainly attribute the weaker baroclinicity to the greater distance of the Kuroshio region to the Asian continent. Even if Pacific cyclones in C3 propagate slightly closer to the Asian continent than those in C2 (Figure 2b,c), these cyclones are still much further away from the continent than all cyclone categories in the North Atlantic (cf. TSS20).

With their reduced importance, low-level baroclinicity and moisture availability alone cannot explain the observed differences in the intensification of cyclones. We therefore also considered the upper-level forcing. The higher intensification of both C2 and C3 cyclones in the Kuroshio region is consistent with their location close to the left exit of an intense upper-tropospheric jet stream (Figure 8d–i), a position favourable for cyclone intensification. The forced ascent at the left exit of the jet likely also contributes to the higher observed precipitation for C2.

Overall, our feature-based analysis identified several mechanisms leading to cyclone intensification that allowed us to estimate the relative contribution of the SST front to the evolution of these cyclones. We highlighted the importance of both the upper-level jet and low-level baroclinicity for cyclone intensification in the Kuroshio region. The propagation of C2 cyclones near the left exit region of the jet can explain both the higher cyclone intensification and increased large-scale precipitation compared with the Atlantic region, despite the more limited moisture availability in the Kuroshio region. Even though our results do not suggest a direct impact of the SST front on the intensification of cyclones, we suggest that the higher baroclinicity observed for cyclones in C3 is partially attributable to the SST front, providing a conducive environment for cyclone growth. We did not find a clear signal of land–sea contrast in the low-level baroclinicity in the Kuroshio region and thus conclude that the land–sea contrast is less effective in providing low-level baroclinicity in the Kuroshio region compared with the Gulf Stream region.

ORCID

Leonidas Tsopouridis https://orcid.org/0000-0002-2043-0871
Clemens Spensberger https://orcid.org/0000-0002-9649-6957
Thomas Spengler https://orcid.org/0000-0002-1747-6385

REFERENCES

Berry, G., Reeder, M.J. and Jakob, C. (2011) A global climatology of atmospheric fronts. *Geophysical Research Letters*, 38, L04809.

Brayshaw, D.J., Hoskins, B. and Blackburn, M. (2009) The basic ingredients of the North Atlantic storm track. Part I: Land–sea contrast and orography. *Journal of the Atmospheric Sciences*, 66, 2539–2558.

Chagnon, J.M. and Gray, S.L. (2015) A diabatically generated potential vorticity structure near the extratropical tropopause in three simulated extratropical cyclones. *Monthly Weather Review*, 143, 2337–2347.

Cione, J.J., Raman, S. and Pietrafesa, L.J. (1993) The effect of Gulf Stream-induced baroclinicity on U.S. East Coast winter cyclones. *Monthly Weather Review*, 121, 421–430.

Dee, D.P., Uppala, S.M., Simmons, A.J., Berrisford, P., Poli, P., Kobayashi, S., Andrae, U., Balmaseda, M.A., Balsamo, G., Bauer, P., Bechtold, P., Beljaars, A.C.M., van de Bergd, L., Bidlot, J., Bormann, N., Delsol, C., Dragani, R., Fuentes, M., Geer, A.J., Haimberger, L., Healy, S.B., Hersbach, H., Holm, E.V., Isaksen, L., Kållberg, P., Köhler, M., M, M., McNally, A.P., Monge-Sanz, B.M., Morcrette, J.-J., Park, B.-K., Peubey, C., de Rosnay, P., Tavolato, C., Thepaut, J.-N. and Vitart, F. (2011) The ERA-Interim reanalysis: configuration and performance of the data assimilation system. *Quarterly Journal of the Royal Meteorological Society*, 137, 553–587.

Fink, A.H., Pohle, S., Pinto, J.G. and Knippertz, P. (2012) Diagnosing the influence of diabatic processes on the explosive deepening of extratropical cyclones. *Geophysical Research Letters*, 39(7), https://doi.org/10.1029/2012GL051025.

Guishard, M.P., Evans, J.L. and Hart, R.E. (2009) Atlantic subtropical storms. Part II: Climatology. *Journal of Climate*, 22, 3574–3594.

Hand, R., Keenlyside, N., Omrani, N.-E. and Latif, M. (2014) Simulated response to inter-annual SST variations in the Gulf Stream region. *Climate Dynamics*, 42, 715–731.

Hirata, H., Kawamura, R., Kato, M. and Shinoda, T. (2018) A positive feedback process related to the rapid development of an extratropical cyclone over the Kuroshio/Kuroshio Extension. *Monthly Weather Review*, 146, 417–433.

Hoskins, B.J. and Hodges, K.I. (2002) New perspectives on the Northern Hemisphere winter storm tracks. *Journal of the Atmospheric Sciences*, 59, 1041–1061.

Hotta, D. and Nakamura, H. (2011) On the significance of sensible heat supply from the ocean in the maintenance of mean baroclinicity along storm tracks. *Journal of Climate*, 24, 3377–3401.

Inatsu, M., Mukougawa, H. and Xie, S.-P. (2000) Formation of subtropical westerly jet core in an idealized GCM without mountains. *Geophysical Research Letters*, 27, 529–532.

Iwao, K., Inatsu, M. and Kimoto, M. (2012) Recent changes in explosively developing extratropical cyclones over the winter Northwestern Pacific. *Journal of Climate*, 25, 7282–7296.

Jacobs, N., Raman, S., Lackmann, G. and Childs, P., Jr. (2008) The influence of the Gulf Stream induced SST gradients on the US East Coast winter storm of 24–25 January 2000. *International Journal of Remote Sensing*, 29, 6145–6174.

Jaffe, S.C., Martin, J.E., Vimont, D.J. and Lorenz, D.J. (2011) A synoptic climatology of episodic, subseasonal retractions of the Pacific jet. *Journal of Climate*, 24, 2846–2860.

Jenkner, J., Sprenger, M., Schwenk, I., Schwierz, C., Dierer, S. and Leuenberger, D. (2010) Detection and climatology of fronts in a high-resolution model reanalysis over the Alps. *Meteorological Applications*, 17, 1–18.

Josey, S.A., Kent, E.C. and Taylor, P.K. (1998) *The Southampton Oceanography Centre (SOC) Ocean–Atmosphere Heat, Momentum and Freshwater Flux Atlas*. Southampton, UK: Southampton Oceanography Centre.

Kuo, Y.-H., Shapiro, M.A. and Donall, E.G. (1991) The interaction between baroclinic and diabatic processes in a numerical simulation of a rapidly intensifying extratropical marine cyclone. *Monthly Weather Review*, 119, 368–384.

Kuwano-Yoshida, A. and Asuma, Y. (2008) Numerical study of explosively developing extratropical cyclones in the northwestern Pacific region. *Monthly Weather Review*, 136, 712–740.

Masunaga, R., Nakamura, H., Miyasaka, T., Nishii, K. and Tanimoto, Y. (2015) Separation of climatological imprints of the Kuroshio Extension and Oyashio Fronts on the wintertime atmospheric boundary layer: their sensitivity to SST resolution prescribed for atmospheric reanalysis. *Journal of Climate*, 28, 1764–1787.

Michel, C., Terpstra, A. and Spengler, T. (2018) Polar mesoscale cyclone climatology for the Nordic Seas based on ERA-Interim. *Journal of Climate*, 31, 2511–2532.

Minobe, S., Kuwano-Yoshida, A., Komori, N., Xie, S.-P. and Small, R.J. (2008) Influence of the Gulf Stream on the troposphere. *Nature*, 452, 206–210.

Murray, R.J. and Simmonds, I. (1991a) A numerical scheme for tracking cyclone centres from digital data. Part I: development and operation of the scheme. *Australian Meteorological Magazine*, 39, 155–166.

Murray, R.J. and Simmonds, I. (1991b) A numerical scheme for tracking cyclone centres from digital data. Part II: application to January and July general circulation model simulations. *Australian Meteorological Magazine*, 39, 167–180.

Nakamura, H. (1992) Midwinter suppression of baroclinic wave activity in the Pacific. *Journal of the Atmospheric Sciences*, 49, 1629–1642.

Nakamura, H., Sampe, T., Goto, A., Ohfuchi, W. and Xie, S.-P. (2008) On the importance of midlatitude oceanic frontal zones for the mean state and dominant variability in the tropospheric circulation. *Geophysical Research Letters*, 35(15), https://doi.org/10.1029/2008GL034010.

Nakamura, H., Sampe, T., Tanimoto, Y. and Shimpo, A. (2004) Observed associations among storm tracks, jet streams and midlatitude oceanic fronts. *Geophysical Monograph Series*, 147, 329–345.

Nakamura, M. and Yamane, S. (2009) Dominant anomaly patterns in the near-surface baroclinicity and accompanying anomalies in the atmosphere and oceans. Part I: North Atlantic basin. *Journal of Climate*, 22, 880–904.

Nuss, W.A. and Anthes, R.A. (1987) A numerical investigation of low-level processes in rapid cyclogenesis. *Monthly Weather Review*, 115, 2728–2743.

Ogawa, F. and Spengler, T. (2019) Prevailing surface wind direction during air–sea heat exchange. *Journal of Climate*, 32, 5601–5617.

Oruba, L., Lapeyre, G. and Rivière, G. (2013) On the poleward motion of midlatitude cyclones in a baroclinic meandering jet. *Journal of the Atmospheric Sciences*, 70, 2629–2649.

Papritz, L. and Spengler, T. (2015) Analysis of the slope of isentropic surfaces and its tendencies over the North Atlantic. *Quarterly Journal of the Royal Meteorological Society*, 141, 3226–3238.

Parfitt, R., Czaja, A., Minobe, S. and Kuwano-Yoshida, A. (2016) The atmospheric frontal response to SST perturbations in the Gulf Stream region. *Geophysical Research Letters*, 43, 2299–2306.

Petterssen, S. and Smebye, S.J. (1971) On the development of extratropical cyclones. *Quarterly Journal of the Royal Meteorological Society*, 97, 457–482.

Pfahl, S., O'Gorman, P.A. and Singh, M.S. (2015) Extratropical cyclones in idealized simulations of changed climates. *Journal of Climate*, 28, 9373–9392.

Pfahl, S. and Sprenger, M. (2016) On the relationship between extratropical cyclone precipitation and intensity. *Geophysical Research Letters*, 43, 1752–1758.

Reed, R.J. and Albright, M.D. (1986) A case study of explosive cyclogenesis in the eastern Pacific. *Monthly Weather Review*, 114, 2297–2319.

Reed, R.J., Grell, G.A. and Kuo, Y.-H. (1993) The Erica IOP 5 storm. Part II: Sensitivity tests and further diagnosis based on model output. *Monthly Weather Review*, 121, 1595–1612.

Riehl, H., Alaka, M., Jordan, C. and Renard, R. (1954) The jet stream in relation to middle latitude cyclones. In: *The Jet Stream*, pp. 38–47. Boston, MA: Springer.

Ritchie, E.A. and Elsberry, R.L. (2003) Simulations of the extratropical transition of tropical cyclones: contributions by the midlatitude upper-level trough to reintensification. *Monthly Weather Review*, 131, 2112–2128.

Riviere, G. and Joly, A. (2006) Role of the low-frequency deformation field on the explosive growth of extratropical cyclones at the jet exit. Part II: Baroclinic critical region. *Journal of the Atmospheric Sciences*, 63, 1982–1995.

Roebber, P.J. (1989) On the statistical analysis of cyclone deepening rates. *Monthly Weather Review*, 117, 2293–2298.

Rudeva, I. and Gulev, S.K. (2011) Composite analysis of North Atlantic extratropical cyclones in NCEP–NCAR reanalysis data. *Monthly Weather Review*, 139, 1419–1446.

Sanders, F. (1986) Explosive cyclogenesis in the west-central North Atlantic Ocean, 1981–84. Part I: Composite structure and mean behavior. *Monthly Weather Review*, 114, 1781–1794.

Sanders, F. and Gyakum, J.R. (1980) Synoptic–dynamic climatology of the "bomb". *Monthly Weather Review*, 108, 1589–1606.

Schemm, S., Rudeva, I. and Simmonds, I. (2015) Extratropical fronts in the lower troposphere–global perspectives obtained from two automated methods. *Quarterly Journal of the Royal Meteorological Society*, 141, 1686–1698.

Schultz, D.M., Keyser, D. and Bosart, L.F. (1998) The effect of large-scale flow on low-level frontal structure and evolution in midlatitude cyclones. *Monthly Weather Review*, 126, 1767–1791.

Sinclair, M.R. and Revell, M.J. (2000) Classification and composite diagnosis of extratropical cyclogenesis events in the southwest Pacific. *Monthly Weather Review*, 128, 1089–1105.

Spensberger, C. and Spengler, T. (2020) Feature-based jet variability in the upper troposphere. *Journal of Climate*, 33(16), 6849–6871.

Spensberger, C., Spengler, T. and Li, C. (2017) Upper-tropospheric jet axis detection and application to the boreal winter 2013/14. *Monthly Weather Review*, 145, 2363–2374.

Tozuka, T., Ohishi, S. and Cronin, M.F. (2018) A metric for surface heat flux effect on horizontal sea-surface temperature gradients. *Climate Dynamics*, 51, 547–561.

Tsopouridis, L., Spensberger, C. and Spengler, T. (2020) Characteristics of cyclones following different pathways in the Gulf Stream region. *Quarterly Journal of the Royal Meteorological Society*. https://doi.org/10.1002/qj.3924.

Uccellini, L.W. (1990) Processes contributing to the rapid development of extratropical cyclones. In: *Extratropical Cyclones*, pp. 81–105: Boston, MA: Springer.

Uccellini, L.W., Kocin, P.J., Petersen, R.A., Wash, C.H. and Brill, K.F. (1984) The Presidents' Day cyclone of 18–19 February 1979: synoptic overview and analysis of the subtropical jet streak influencing the pre-cyclogenetic period. *Monthly Weather Review*, 112, 31–55.

Vannière, B., Czaja, A. and Dacre, H.F. (2017) Contribution of the cold sector of extratropical cyclones to mean state features over the Gulf Stream in winter. *Quarterly Journal of the Royal Meteorological Society*, 143, 1990–2000.

Wang, C.-C. and Rogers, J.C. (2001) A composite study of explosive cyclogenesis in different sectors of the North Atlantic. Part I: cyclone structure and evolution. *Monthly Weather Review*, 129, 1481–1499.

Wang, L., Hu, H. and Yang, X. (2019) The atmospheric responses to the intensity variability of subtropical front in the wintertime north Pacific. *Climate Dynamics*, 52, 5623–5639.

Yanase, W. and Niino, H. (2019) Parameter sweep experiments on a spectrum of cyclones with diabatic and baroclinic processes. *Journal of the Atmospheric Sciences*, 76, 1917–1935.

Yanase, W., Niino, H., Hodges, K. and Kitabatake, N. (2014) Parameter spaces of environmental fields responsible for cyclone development from tropics to extratropics. *Journal of Climate*, 27, 652–671.

Yao, Y., Zhong, Z. and Yang, X.-Q. (2016) Numerical experiments of the storm track sensitivity to oceanic frontal strength within the Kuroshio/Oyashio extensions. *Journal of Geophysical Research: Atmospheres*, 121, 2888–2900.

Yoshida, A. and Asuma, Y. (2004) Structures and environment of explosively developing extratropical cyclones in the northwestern Pacific region. *Monthly Weather Review*, 132, 1121–1142.

APPENDIX

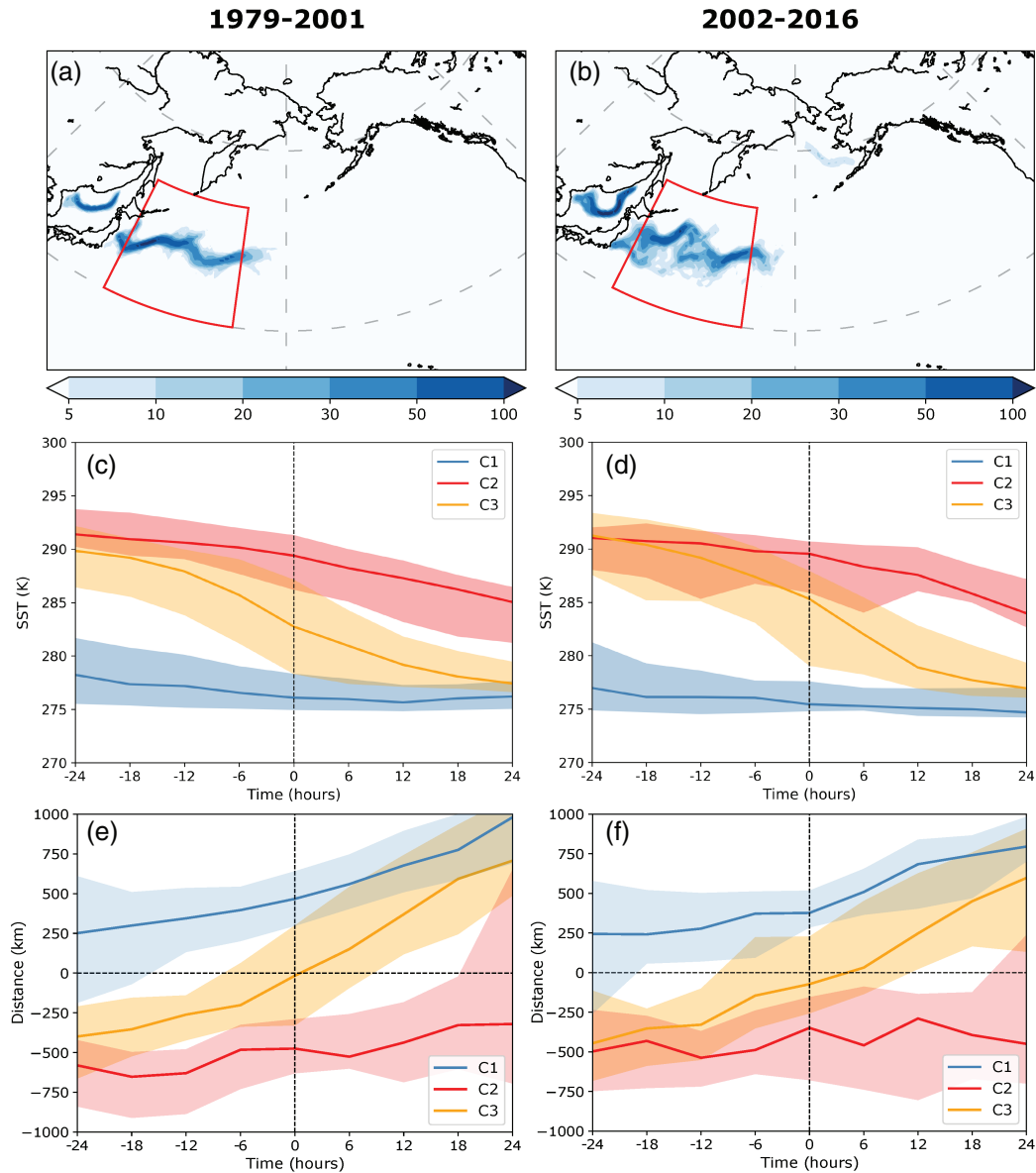Figure A1 shows the distribution of SST and SST fronts prior to and after the ERA-Interim resolution change.

FIGURE A1 (a) Density of SST fronts (km of line $(100\,km)^{-2}$) for the winter seasons in 1979–2001 for the North Pacific. The Kuroshio region is marked with a red box. (b) As (a), but for 2002–2016. (c) SST (K) for the three categories relative to the time of maximum intensification for the winter seasons in 1979–2001. Lines indicate the median and the shading the interquartile range. (d) As (c), but for 2002–2016. (e) Distance (km) between cyclone centres and the SST front relative to the time of maximum intensification for the winter seasons in 1979–2001. (f) As (e), but for 2002–2016